UC Irvine
UC Irvine Previously Published Works

Title

Time-Domain Green's Function for an Infinite Sequentially Excited Periodic Planar Array of Dipoles

Permalink

Journal

ISSN

Authors

Capolino, Filippo
Felsen, Leopold B

Publication Date

DOI

Copyright Information

Peer reviewed

Time-Domain Green's Function for an Infinite Sequentially Excited Periodic Planar Array of Dipoles

Filippo Capolino, *Member, IEEE,* and Leopold B. Felsen, *Life Fellow, IEEE*

Abstract—The present paper is a continuation of previous explorations by the authors, aimed at gaining a basic understanding of the time domain (TD) behavior of large periodic phased (i.e., sequentially turned-on) array antenna and related configurations. Our systematic investigation of the relevant canonical TD dipole-excited Green's functions has so far included those for infinite and truncated sequentially pulsed *line* periodic arrays, parameterized in terms of radiating (propagating) and nonradiating (evanescent) *conical* TD Floquet waves (FW) and truncation-induced TD FW-modulated tip diffractions. The present contribution extends these investigations to an infinite periodic sequentially pulsed *planar* array, which generates pulsed *plane* propagating and evanescent FW. Starting from the familiar frequency domain (FD) transformation of the linearly phased element-by-element summation synthesis into summations of propagating and evanescent FWs, we access the time domain by Fourier inversion. The inversion integrals are manipulated in a unified fashion into exact closed forms, which are parameterized by the single nondimensional quantity $\eta = c/v_{u1}^{(p)}$, where $v_{u1}^{(p)}$ and c are the excitation phase speed along a preferred phasing direction u_1 in the array plane and the ambient wave speed, respectively. The present study deals with the practically relevant rapidly phased propagating case $\eta < 1$, reserving the more intricate slowly phased $\eta > 1$ regime for a future manuscript. Numerical reference data generated via element-by-element summation over the fields radiated by the individual dipoles with ultrawide band-limited excitation are compared with results obtained much more efficiently by inclusion of a few TD–FWs. Physical interpretation of the formal TD–FW solutions is obtained by recourse to asymptotics, instantaneous frequencies and wavenumbers, and related constructs. Of special interest is the demonstration that the TD–FWs emerge along "equal-delay" ellipses from the array plane; this furnishes a novel and physically appealing interpretation of the planar array TD–FW phenomenology.

Index Terms—Antenna arrays, arrays, floquet waves, Green's function, periodic structures, time-domain (TD) analysis, transient analysis.

F. Capolino was with the Department of Information Engineering, University of Siena, 53100 Siena, Italy. He is now with the Department of Electric and Computer Engineering, University of Houston, TX 77004 USA.

L. B. Felsen is with the Department of Aerospace and Mechanical Engineering and the Department of Electrical and Computer Engineering, Boston University, Boston, MA 02215 USA, and is also with the Polytechnic University, Brooklyn, NY 11201 USA (e-mail: lfelsen@bu.edu).

I. INTRODUCTION

THIS paper represents the third in a series of prototype studies [1], [2] of the time-domain (TD) behavior of sequentially excited periodic dipole array configurations, motivated by similar investigations in the frequency domain (FD) [3]–[6], which have already been applied effectively and efficiently to finite practical array antennas [7]–[10]. Referring to the more detailed introduction in [1] for background, we proceed in Section II to the formulation of the problem in terms of the frequency-domain (FD) and time-domain (TD) fields excited by the individual phased dipole radiators. Via Poisson summation, these discretely spaced individual FD and TD sources are reexpressed collectively in terms of equivalent global periodicity-induced continuous distributions which obey the Floquet wave (FW) dispersion relation and span the entire array surface. The FD-FW and TD–FW wavefields, i.e., the Floquet plane waves, radiated by these FW-modulated aperture distributions are developed in Sections III and IV, respectively, with emphasis in the TD on the new phenomenologies exhibited by the planar array, as well as on similarities with the previously investigated TD-infinite line dipole array [1]. As previously cited in [1], the TD–FW fields are found to be expressible in new exact closed forms which reduce to known results for special choices of the problem parameters. Numerical results in Section V furnish reference data which are used for comparison with considerably more efficient FW-generated fields. Conclusions are presented in Section VI.

II. STATEMENT OF THE PROBLEM

A. Element-by-Element Formulation

The geometry of the planar array of dipoles oriented along the $\mathbf{J}_0$ direction and excited by transient currents in free space is shown in Fig. 1. The period of the array is d_1 and d_2 in the x_1 and x_2 directions, respectively. The vector electric field is simply related to the $\mathbf{J}_0$ directed magnetic scalar potential A which shall be used throughout. A caret ($\wedge$) tags time-dependent quantities; boldface symbols define vector quantities; $\boldsymbol{i}_{x1}$, $\boldsymbol{i}_{x2}$, and $\boldsymbol{i}_z$ denote unit vectors along x_1, x_2, and z, respectively. FD and TD quantities are related by the Fourier transform pair

$$A(\mathbf{r}, \omega) = \int_{-\infty}^{\infty} \hat{A}(\mathbf{r}, t) e^{-j\omega t} dt,$$

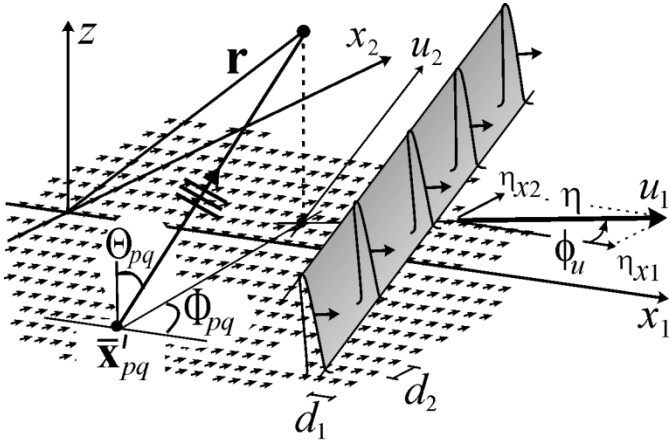$$\hat{A}(\mathbf{r}, t) = \frac{1}{2\pi} \int_{-\infty}^{\infty} A(\mathbf{r}, \omega) e^{j\omega t} d\omega. \tag{1}$$

Fig. 1. Planar periodic array of dipoles. Physical configuration and coordinates. d_1, d_2: interelement spacing along x_1 and x_2, respectively; $\omega\gamma_{u_1} = k\eta$: phase gradient of the excitation (i.e., the wavefront) along the direction i_{u_1}; $\gamma_{u_1} = \eta/c$: "slowness" (normalized wavenumber) along i_{u_1}; $v_{u_1}^{(p)} = c/\eta = 1/\gamma_{u_1}$: phase speed along i_{u_1}.

The phased array FD and TD dipole currents $J(\omega)$ and $\hat{J}(t)$, respectively, are given by

$$\left.\begin{array}{c} J(\omega) \\ \hat{J}(t) \end{array}\right\} = \sum_{m=-\infty}^{\infty} \sum_{n=-\infty}^{\infty} \delta(\mathbf{x}' - \mathbf{x}_{mn})$$
$$\times \left\{\begin{array}{c} e^{-jn k \boldsymbol{i}_{u_1} \cdot \mathbf{x}_{mn}} \\ \delta\left(t - \dfrac{\eta \boldsymbol{i}_{u_1} \cdot \mathbf{x}_{mn}}{c}\right) \end{array}\right\} \quad (2)$$

$$\boldsymbol{i}_{u_1}\eta = \eta_{x1}\boldsymbol{i}_{x1} + \eta_{x2}\boldsymbol{i}_{x2} \quad (3)$$

where $\mathbf{x}_{mn} = md_1\boldsymbol{i}_{x1} + nd_2\boldsymbol{i}_{x2}$ is the mnth dipole location, $\delta(\mathbf{x}' - \mathbf{x}_{mn}) = \delta(x_1' - md_1)\delta(x_2' - nd_2)$, $k = \omega/c$ denotes the ambient wavenumber, and c denotes the ambient wave speed. Moreover, $\omega\eta_{x1}/c$ and $\omega\eta_{x2}/c$, with

$$\eta_{x1} = \eta\cos\phi_{u_1}, \quad \eta_{x2} = \eta\sin\phi_{u_1} \quad (4)$$

are the interelement phase gradients along x_1 and x_2, respectively. Here, η is chosen to match the form $\eta = c\gamma$ of the important nondimensional parameter introduced previously [1]. This yields

$$\eta = c\gamma_{u_1} = \frac{c}{v_{u_1}^{(p)}} \quad (5)$$

with $\gamma_{u_1} = \eta/c = 1/v_{u_1}^{(p)}$ now denoting the normalized (with respect to ω) phase gradient, and $v_{u_1}^{(p)} = c/\eta$ the corresponding impressed phase speed, along the array in the $\boldsymbol{i}_{u_1}$ direction (see Fig. 1). The FD phasing unit vector $\boldsymbol{i}_{u_1}$ is rotated through the angle ϕ_u with respect the x_1 axis; this corresponds in the TD to sequentially pulsed dipole elements, with the element at $\mathbf{x} = \mathbf{x}_{mn}$ turned on at time $t_{mn} = \eta\boldsymbol{i}_{u_1} \cdot \mathbf{x}_{mn}/c$. Choosing the normalized form for η along $\boldsymbol{i}_{u_1}$ as in (5) systematizes subsequent notation and interpretation.

The respective regimes $\eta < 1$ and $\eta > 1$ characterize two distinct TD wave phenomenologies with phase speeds c/η along u_1 larger or smaller than the ambient wave speed c. Only the practically more important $\eta < 1$ regime is examined in this paper.

B. Collective Formulation

To convert the individual element contributions in (2) into equivalent collective smooth aperture distributions, we use the Poisson sum formula in its most elementary form given by $\sum_{n=-\infty}^{\infty} \delta(x - nd) = d^{-1} \sum_{q=-\infty}^{\infty} \exp(-j2\pi qx/d)$ [11, pp. 117] . When applied sequentially to the double infinite series of phased m, n-indexed FD and TD elements in (2), Poisson summation yields

$$\sum_{m,n=-\infty}^{\infty} \left\{\begin{array}{c} e^{-jn k \boldsymbol{i}_{u_1} \cdot \mathbf{x}_{mn}} \\ \delta\left(t - \dfrac{\eta \boldsymbol{i}_{u_1} \cdot \mathbf{x}_{mn}}{c}\right) \end{array}\right\} \delta(\mathbf{x}' - \mathbf{x}_{mn})$$
$$= \frac{1}{d_1 d_2} \sum_{p,q=-\infty}^{\infty} \left\{\begin{array}{c} e^{-j\mathbf{k}_{t,pq}\cdot\mathbf{x}'} \\ e^{-j(\boldsymbol{\alpha}_{pq}\cdot\mathbf{x}')}\delta\left(t - \dfrac{\eta\boldsymbol{i}_{u_1}\cdot\mathbf{x}'}{c}\right) \end{array}\right\} \quad (6)$$

The vector wavenumber

$$\mathbf{k}_{t,pq}(\omega) = k_{x1,q}\boldsymbol{i}_{x1} + k_{x1,q}\boldsymbol{i}_{x2} = \eta k\boldsymbol{i}_{u_1} + \boldsymbol{\alpha}_{pq}, \quad (7)$$

$$\boldsymbol{\alpha}_{pq} = \alpha_{1,q}\boldsymbol{i}_{x1} + \alpha_{2,p}\boldsymbol{i}_{x_1 x_2} \quad (8)$$

which combines the two Floquet-type dispersion relations

$$k_{x1,q}(\omega) = \eta k\cos\phi_u + \alpha_{1,q}, \quad \alpha_{1,q} = \frac{2\pi q}{d_1} \quad (9)$$

$$k_{x2,p}(\omega) = \eta k\sin\phi_u + \alpha_{2,p}, \quad \alpha_{2,p} = \frac{2\pi p}{d_2} \quad (10)$$

with $p, q = 0, \pm1, \pm2, \ldots$, has previously been employed in the FD studies of planar dipole arrays [3]–[5]. The subscript "t" on $\mathbf{k}_{t,pq}$ denotes the vector component transverse to z, and $\boldsymbol{\alpha}_{pq}$ represents the ω-independent part of the vector dispersion relation in (7). Thus, in the frequency domain, Poisson summation converts the effect of the infinite periodic array of *individual phased m, n-indexed dipole* radiators collectively into an infinite superposition of linearly *smoothly phased p, q-indexed* equivalent *planar* distributions that furnish the initial conditions for propagating (i.e., radiating) PFW and evanescent (i.e., nonradiating) EFW Floquet-type waves. In the TD, the m, n-indexed sequentially pulsed dipoles are converted collectively into smoothly phased, p, q-indexed impulsive source distributions $\delta(t - \eta\boldsymbol{i}_{u_1} \cdot \mathbf{x}'/c)$, which travel with phase speed c/η in the $\boldsymbol{i}_{u_1}$ direction, which is the direction of the wavefront shown in Fig. 1.

III. FLOQUET WAVES: FREQUENCY DOMAIN

To obtain for the potential fields $A_{mn}(\mathbf{r},\omega)$ radiated by the linearly phased dipole array element currents at $\mathbf{x}_{mn}$ an equivalent sum of FW potentials $A_{pq}^{\text{FW}}(\mathbf{r},\omega)$ radiated by the smoothly phased FW-modulated aperture distributions, we multiply the FD portion of (6) by the FD element Green's function

$$A(\mathbf{r},\mathbf{x}',\omega) = \frac{e^{-jkR(\mathbf{x}')}}{4\pi R(\mathbf{x}')}, \quad R(\mathbf{x}') = \sqrt{|\mathbf{x} - \mathbf{x}'|^2 + z^2} \quad (11)$$

and perform the integration $\int_{-\infty}^{\infty} dx_i'$, for $i = 1$ and 2, to generate $A_{mn} = A(\mathbf{r},\mathbf{x}_{mn},\omega)\exp(-jn\eta\boldsymbol{i}_{u_1} \cdot \mathbf{x}_{mn}/c)$ on the left-hand side (LHS) of (6). Here, $\mathbf{r} = \mathbf{x} + z\boldsymbol{i}_z$ denotes the position vector. On the right-hand side (RHS) of (6), this yields the collective

FW-phased plane waves (it is the inverse of the transform shown in [12, p. 481])

$$
\begin{aligned}
A_{pq}^{\text{FW}}(\mathbf{r}, \omega) &= \frac{1}{d_1 d_2} \int_{-\infty}^{\infty} \int_{-\infty}^{\infty} \frac{e^{-jkR(\mathbf{x}')}}{4\pi R(\mathbf{x}')} \\
&\quad \times e^{-j\mathbf{k}_{t,pq} \cdot \mathbf{x}'} dx_1' dx_2' \\
&= \frac{e^{-j\mathbf{k}_{pq}^{\text{FW}} \cdot \mathbf{r}}}{2jd_1 d_2 k_{zpq}}.
\end{aligned}
\tag{12}
$$

Here, $\mathbf{k}_{pq}^{\text{FW}} = \mathbf{k}_{t,pq} + k_{zpq}\hat{\mathbf{z}}$ denotes the total FW_{pq} propagation vector, and

$$
k_{zpq}(\omega) = \sqrt{k^2 - k_{x1,q}^2 - k_{x2,p}^2} = \sqrt{k^2 - |\mathbf{k}_{t,pq}|^2} \tag{13}
$$

is the wavenumber along z. The square root function in (13) is defined so that $\Im m k_{zpq} \leq 0$ on the top Riemann sheet, consistent with the radiation condition at $z = \infty$. Furthermore, $\Re e k_{zpq} \geq 0$ or ≤ 0 for $\omega > 0$ or < 0, respectively, in order to satisfy the radiation condition for positive and negative real frequencies. In (12), Floquet waves with transverse propagation constants $k_{t,pq} < k$ or $k_{t,pq} > k$, where $k_{t,pq} = |\mathbf{k}_{t,pq}| = (k_{x1,q}^2 + k_{x2,p}^2)^{1/2}$, characterize PFW or EFW, respectively, *along* z. Note that by phase matching along x_1, x_2, each PFW contributes at the observation point $\mathbf{r} \equiv (x_1, x_2, z)$ a ray asymptotic field originating at a point $\bar{\mathbf{x}}_{pq}' = \mathbf{x} - (z/k_{z,pq})\mathbf{k}_{t,pq}$ on the (x_1, x_2)-plane. The ray emanating from the point $\bar{\mathbf{x}}_{pq}'$ lie on a ray with angular displacement Θ_{pq} from the z-axis, and azimuthal displacement Φ_{pq} from the x_1 axis (see Fig. 1),

$$
\Theta_{pq} = \cos^{-1}\left(\frac{k_{zpq}}{k}\right), \quad \Phi_{pq} = \tan^{-1}\left(\frac{k_{x2,p}}{k_{x1,q}}\right) \tag{14}
$$

for positive or negative frequencies. For $p \neq 0$ or $q \neq 0$, $\omega > 0$ and $\omega < 0$ give rise to two different FW_{pq} propagation angles. When $k_{t,pq} = \sqrt{k_{x1,q}^2 + k_{x2,p}^2}$ approaches k, the polar angle Θ_{pq} tends to $\pi/2$. Beyond that limit, when $k_{t,pq} > k$, the polar angle becomes complex and the field becomes evanescent along z, with $k_{t,pq} = k$, i.e., $k_{zpq} = 0$, defining the pqth FW cutoff condition. Owing to the exponential attenuation of EFW_{pq} along z, the EFW portion of $\sum_{pq=-\infty}^{\infty} A_{pq}^{\text{FW}}$ converges rapidly away from the array plane and a few terms may suffice for an adequate approximation of the total radiated field.

IV. FLOQUET WAVES: TIME DOMAIN

Three distinct approaches are analyzed, each describing different aspects of TD–FWs. The first two lead to exact expressions for TD–FWs, while the third leads to an asymptotic description of the same phenomena.

A. Fourier Inversion From the FD

The TD Floquet Wave is obtained through Fourier inversion from the frequency domain

$$
\begin{aligned}
\hat{A}_{pq}^{\text{FW}}(\mathbf{r}, t) &= \frac{1}{2\pi} \int_{-\infty}^{\infty} A_{pq}^{\text{FW}}(\mathbf{r}, \omega) e^{j\omega t} d\omega \\
&= \frac{e^{-j\boldsymbol{\alpha}_{pq} \cdot \mathbf{x}}}{4\pi j d_1 d_2} \int_{-\infty}^{\infty} \frac{e^{-jk_{zpq}(\omega)z}}{k_{zpq}(\omega)} e^{j\omega\tau} d\omega
\end{aligned}
\tag{15}
$$

$$
\tau = t - \frac{\eta \boldsymbol{i}_{u_1} \cdot \mathbf{x}}{c} \tag{16}
$$

with $A_{pq}(\mathbf{r}, \omega)$ given in (12). The $k_{zpq}(\omega)$ wavenumber is rewritten as

$$
\begin{aligned}
k_{zpq}(\omega) &= \sqrt{\left(\frac{\omega}{c}\right)^2 (1 - \eta^2) - 2\frac{\omega}{c}\eta \boldsymbol{i}_{u_1} \cdot \boldsymbol{\alpha}_{pq} - \alpha_{pq}^2} \\
&= \sqrt{\left[\omega'^2 - \tilde{\omega}_{pq}^2\right] \frac{(1 - \eta^2)}{c^2}},
\end{aligned}
\tag{17}
$$

in which we used the frequency shift

$$
\omega' = \omega - \bar{\omega}_{pq} \tag{18}
$$

and the definitions

$$
\bar{\omega}_{pq} = \frac{\eta c}{1 - \eta^2} \boldsymbol{i}_{u_1} \cdot \boldsymbol{\alpha}_{pq}, \tag{19}
$$

$$
\tilde{\omega}_{pq}^2 = \bar{\omega}_{pq}^2 + \frac{c^2}{1 - \eta^2} \alpha_{pq}^2. \tag{20}
$$

Thus, (15) becomes

$$
\begin{aligned}
\hat{A}_{pq}^{\text{FW}}(\mathbf{r}, t) &= \frac{c e^{j(\bar{\omega}_{pq}\tau - \boldsymbol{\alpha}_{pq} \cdot \mathbf{x})}}{4\pi j d_1 d_2} \\
&\quad \times \int_{-\infty}^{\infty} \frac{e^{-j\sqrt{(\omega'2 - \tilde{\omega}_{pq}^2)(1-\eta^2)}z/c}}{\sqrt{(\omega'^2 - \tilde{\omega}_{pq}^2)(1 - \eta^2)}} e^{j\omega'\tau} d\omega'
\end{aligned}
\tag{21}
$$

The integrand has branch points at $\omega' = \pm\tilde{\omega}_{pq}$, with [from (20)]

$$
\tilde{\omega}_{pq} = \frac{c}{1 - \eta^2} \sqrt{\alpha_{pq}^2 - \eta^2(\boldsymbol{\alpha}_{pq} \cdot \boldsymbol{i}_{u_2})^2} \tag{22}
$$

as shown in Fig. 2. Cuts are determined by imposing $\Im m[(\omega'^2 - \tilde{\omega}_{pq}^2)(1 - \eta^2)/c]^{1/2} \leq 0$ on the top ω'-plane Riemann sheet, and $\Re e[(\omega'^2 - \tilde{\omega}_{pq}^2)(1 - \eta^2)/c]^{1/2} \geq 0$ or ≤ 0 for $\omega > 0$ or $\omega < 0$, respectively, in accord with the definition of k_{zpq} in (13). In the ω'-plane, the vertical dashed line at $\omega' = -\bar{\omega}_{pq}(\omega = 0)$ separates positive and negative ω frequencies (only $\bar{\omega}_{pq} > 0$ is shown in the figure).

Defining

$$
\tau_0 = \sqrt{1 - \eta^2} \frac{z}{c} \tag{23}
$$

Equation (21) is rewritten as

$$
\begin{aligned}
\hat{A}_{pq}^{\text{FW}}(\mathbf{r}, t) &= \frac{c e^{j(\bar{\omega}_{pq}\tau - \boldsymbol{\alpha}_{pq} \cdot \mathbf{x})}}{4\pi j d_1 d_2 \sqrt{1 - \eta^2}} \\
&\quad \times \int_{-\infty}^{\infty} \frac{e^{-j\tau_0\sqrt{\omega'^2 - \tilde{\omega}_{pq}^2}}}{\sqrt{\omega'^2 - \tilde{\omega}_{pq}^2}} e^{j\omega'\tau} d\omega'
\end{aligned}
\tag{24}
$$

with $\Im m\sqrt{\omega'^2 - \tilde{\omega}_{pq}^2} \leq 0$ and $\Re e\sqrt{\omega'^2 - \tilde{\omega}_{pq}^2} \geq 0$ or ≤ 0 for $\omega > 0$ or $\omega < 0$, respectively, in accord with the definitions for k_{zpq} in (13). The positive–negative ω transition at $\omega' = -\bar{\omega}_{pq}$ occurs between the two branch points. The indentation of the integration path in (24) is chosen in accord with the radiation condition at ∞ (causality) for any ω; therefore, the integration path from $-\infty$ to $+\infty$ is shifted below the branch cuts (see Fig. 2), where $\Re e (\omega'^2 - \tilde{\omega}^2)^{1/2} \geq 0$ or ≤ 0 for $\omega > 0$ or $\omega < 0$ in accord with the radiation condition specified in the text after (13) (see also [12, p. 35] where, to ensure the existence of the Fourier pair in (1), the ω' variable and therefore the contour of integration in (24) is shifted slightly below the real ω' axis into $\Im m\omega' < 0$).
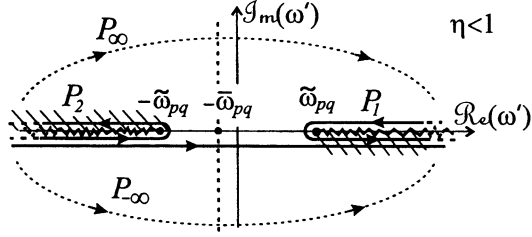
Fig. 2.   Topology of the complex ω'-plane. Branch points are located at $\omega' = \pm\tilde{\omega}_{pq}$. The vertical dotted line at $\omega' = -\bar{\omega}_{pq}$ ($\omega = 0$) separates positive and negative ω frequencies (here, $\bar{\omega}_{pq} > 0$ for simplicity). The dashed region denotes the side of the cuts where $\Re e(\omega'^2 - \tilde{\omega}_{pq}^2)^{1/2} > 0$, according to the choice of the root for $k_{z_{pq}}$ in (13). For Fourier inversion (see (1)), the integration path is moved to the real axis and indented accordingly with respect to the singularities.

Since for $\tau < \tau_0$, the integrand in (24) decays exponentially in $\Im m\omega' < 0$, the integration contour can be closed by addition of the noncontributing portion $P_{-\infty}$; because no singularities are located within the contour, the integral vanishes by Cauchy's theorem. For $\tau > \tau_0$, the integration contour can be closed by the noncontributing portion P_∞, and is therefore deformable into $P_1 + P_2$. Using the relation (demonstrated in Appendix A)

$$I_i = \int_{P_i} d\omega' e^{j\omega'\tau} \frac{e^{-j\tau_0\sqrt{\omega'^2-\tilde{\omega}_{pq}^2}}}{\sqrt{\omega'^2-\tilde{\omega}_{pq}^2}}$$
$$= \pi j H_0^{(i)}\left[\tilde{\omega}_{pq}\sqrt{\tau^2-\tau_0^2}\right], \quad i=1,2 \qquad (25)$$

in which $H_0^{(1)}$ and $H_0^{(2)}$ are the zeroth-order Hankel functions of the first and second kind, respectively, and combining $J_0(x) = 1/2\left[H_0^{(1)}(x) + H_0^{(2)}(x)\right]$, leads directly to the closed form exact expression

$$\hat{A}_{pq}^{\mathrm{FW}}(\mathbf{r},t) = \frac{ce^{j(\bar{\omega}_{pq}\tau-\boldsymbol{\alpha}_{pq}\cdot\mathbf{x})}}{2d_1 d_2\sqrt{1-\eta^2}}$$
$$\times J_0\left[\tilde{\omega}_{pq}\sqrt{\tau^2-\tau_0^2}\right] U(\tau-\tau_0) \qquad (26)$$

with $U(\tau) = 1$ or 0 for $\tau > 0$ or $\tau < 0$, respectively.

Although obtained by conventional Fourier inversion from the frequency domain, the result in (26) is complex for p or $q \neq 0$ since $\alpha_{pq} \neq 0$ and, from (19), $\bar{\omega}_{pq} \neq 0$ in this case. The phenomenology is directly analogous to that observed previously for the line dipole array [1], and is addressed as in [1] by $(+p, +q)$, $(-p, -q)$ pairing to obtain the "physically observable" *real* TD–FW field. Noting from (8) and (19) that $\alpha_{-p,-q} = -\alpha_{p,q}$ and $\bar{\omega}_{-p,-q} = -\bar{\omega}_{p,q}$, it follows that the "physically observable" *real* TD–FW field is given by

$$\hat{A}_{+p,+q}^{\mathrm{FW}} + \hat{A}_{-p,-q}^{\mathrm{FW}} = 2\Re e \hat{A}_{pq}^{\mathrm{FW}} \qquad (27)$$
$$\Re e \hat{A}_{pq}^{\mathrm{FW}}(\mathbf{r},t) = \frac{c\cos(\boldsymbol{\alpha}_{pq}\cdot\mathbf{x} - \bar{\omega}_{pq}\tau)}{2d_1 d_2\sqrt{1-\eta^2}}$$
$$\times J_0\left[\tilde{\omega}_{pq}\sqrt{\tau^2-\tau_0^2}\right]$$
$$\times U(\tau-\tau_0). \qquad (28)$$

For the $p = q = 0$ mode, one has $\alpha_{pq} = |\boldsymbol{\alpha}_{pq}| = 0$, with $\bar{\omega}_{pq} = 0$ and $\tilde{\omega}_{pq} = 0$; i.e., the argument of the Bessel

function in (26) vanishes. Since $J_0(0) = 1$, we have $\hat{A}_{00}^{\mathrm{FW}} = c\left(2d_1 d_2\sqrt{1-\eta^2}\right)^{-1} U(\tau-\tau_0)$ which agrees exactly with the real field radiated by an impulsively excited smooth infinite plane source with phasing specified by η/c.

B. Spatial Synthesis of TD–FWs Via Poisson Summation

Since the FD-mn series in (6), when applied to A_{mn}, has summands $A_{mn}(\mathbf{r},\omega) = A(\mathbf{r}, \mathbf{x}_{mn}, \omega)\exp(-j\omega\eta\boldsymbol{i}_{u_1}\cdot\mathbf{x}_{mn}/c)$ composed of two ω-dependent functions (see text after (11)), the TD $\hat{A}_{mn}(\mathbf{r},t)$ involves a convolution which yields (29). Alternatively, first, one finds that $\hat{A}(\mathbf{r}, \mathbf{x}', t) = \delta(t - R(\mathbf{x}')/c)/(4\pi R(\mathbf{x}'))$. When this function is time-convolved with the TD portion on the left-hand side of (6), i.e., $\int_{-\infty}^{\infty} dt' A(\mathbf{r}, \mathbf{x}', t-t')\delta(t' - \eta\boldsymbol{i}_{u_1}\cdot\mathbf{x}_{mn}/c)$, followed by $\int_{-\infty}^{\infty}\int_{-\infty}^{\infty} dx_1' dx_2'$, one obtains the field

$$\hat{A}_{mn}(\mathbf{r},t) = \frac{\delta\left(t - \frac{\eta\boldsymbol{i}_{u_1}\cdot\mathbf{x}_{mn}}{c} - \frac{R(\mathbf{x}_{mn})}{c}\right)}{4\pi R(\mathbf{x}_{mn})} \qquad (29)$$

excited by the impulsive mnth dipole current in (2) which represents a spherical impulsive wavefront radiated by the dipole at $\mathbf{x} = \mathbf{x}_{mn}$ at the delayed time $t_{mn} = \eta\boldsymbol{i}_{u_1}\cdot\mathbf{x}_{mn}/c$. The same operations applied to the right-hand side of (6), or direct FD inversion of (12), yields the TD–FW

$$\hat{A}_{pq}^{\mathrm{FW}}(\mathbf{r},t) = \frac{1}{4\pi d_1 d_2}\int_{-\infty}^{\infty}\int_{-\infty}^{\infty}\frac{e^{-j\boldsymbol{\alpha}_{pq}\cdot\mathbf{x}'}}{R(\mathbf{x}')}$$
$$\times\delta\left(t - \frac{\eta\boldsymbol{i}_{u_1}\cdot\mathbf{x}'}{c} - \frac{R(\mathbf{x}')}{c}\right)dx_1' dx_2'. \qquad (30)$$

The argument of the delta function in (30) identifies the two-dimensional (2-D) integral as a Radon slant-stack projection transform [13] (normalized to the unit cell area $d_1 d_2$). The integrand in (30) contributes only for those real (x_1', x_2')-values which satisfy

$$\tau + \eta\frac{\boldsymbol{i}_{u_1}\cdot(\mathbf{x}-\mathbf{x}')}{c} - \frac{R(\mathbf{x}')}{c} = 0$$
$$\tau = t - \frac{\eta\boldsymbol{i}_{u_1}\cdot\mathbf{x}}{c}. \qquad (31)$$

To understand the implications of this condition, we change coordinates to

$$(\mathbf{x}'-\mathbf{x})\cdot\boldsymbol{i}_{u_1} = u_1, \quad (\mathbf{x}'-\mathbf{x})\cdot\boldsymbol{i}_{u_2} = u_2 \qquad (32)$$

with $\boldsymbol{i}_{u_2} = -\sin\phi_u\boldsymbol{i}_{x_1} + \cos\phi_u\boldsymbol{i}_{x_2}$ (see Fig. 1), which orients the u_1 coordinate along the direction of propagation of the traveling impulse excitation (see Figs. 3 and 4). Therefore, the integral in (30) becomes

$$\hat{A}_{pq}^{\mathrm{FW}}(\mathbf{r},t) = \frac{e^{-j\boldsymbol{\alpha}_{pq}\cdot\mathbf{x}}}{4\pi d_1 d_2}\int_{-\infty}^{\infty}\int_{-\infty}^{\infty} e^{-j(\boldsymbol{i}_{u_2}\cdot\boldsymbol{\alpha}_{pq})u_2}$$
$$\cdot\frac{e^{-j\boldsymbol{i}_{u_1}\cdot\boldsymbol{\alpha}_{pq}u_1}}{R(u_1,u_2)}\delta\left(\tau - \frac{\eta u_1}{c} - \frac{R(u_1,u_2)}{c}\right)du_1 du_2 \qquad (33)$$

and (31) is written as

$$\tau - \frac{\eta u_1}{c} - \frac{R(u_1,u_2)}{c} = 0$$
$$R(u_1,u_2) = \sqrt{\rho^2(u_2) + u_1^2}$$
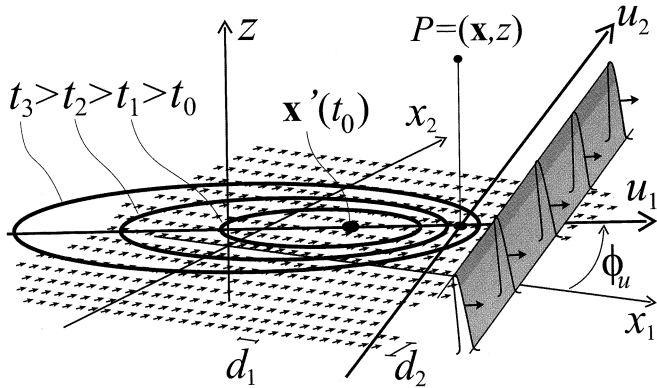$$\rho(u_2) = \sqrt{z^2 + u_2^2}. \qquad (34)$$

Fig. 3. Phenomenology matched coordinate system (u_1, u_2), rotated with respect to (x_1, x_2), whose transformation is given in (32). u_1 points in the direction $\boldsymbol{i}_{u_1} = \cos\phi_u \boldsymbol{i}_{x_1} + \sin\phi_u \boldsymbol{i}_{x_2}$ of the propagating wavefront. The first signal arrival at the observation point $(\mathbf{x}, z)$ originates at the earlier point $\mathbf{x}'(t_0) = x_1'(t_0)\boldsymbol{i}_{x_1} + x_2'(t_0)\boldsymbol{i}_{x_2} \equiv z\eta(1-\eta^2)^{-1/2}\boldsymbol{i}_{u_1}$. Successively, for $t > t_0$, contributions arrive at the observer *simultaneously* from points whose locus is a distinct "equal delay" ellipse (see also, Fig. 4).
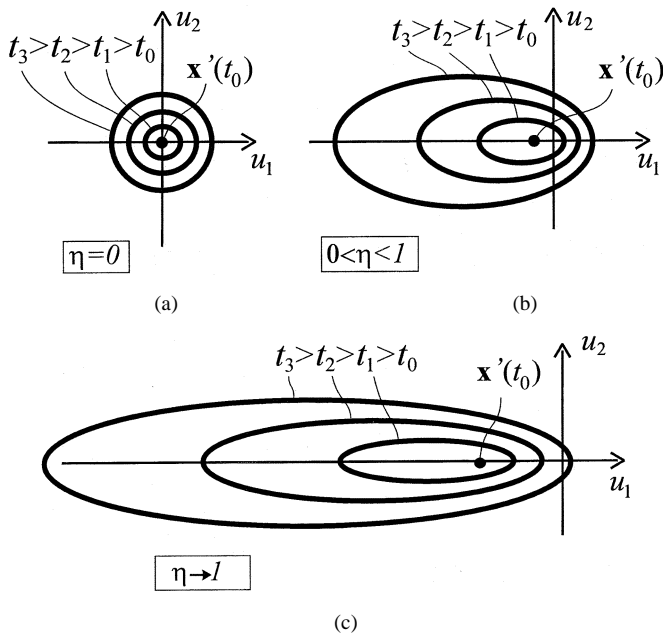

Fig. 4. Various equal delay ellipse configurations, represented in the (u_1, u_2) plane at three time instants $t_3 > t_2 > t_1$, all greater than the turn-on time t_0. The signal arriving at the observer at t_0 is generated earlier at the point $\mathbf{x}'(t_0)$ which, in the (u_1, u_2) plane, is located at $(-z\eta(1-\eta^2)^{-1/2}, 0)$. (a) For $\eta = 0$, ellipses degenerate to circles. (b) For a generic $0 < \eta < 1$, the equal delay ellipses have axis ratio equal to $1/(1-\eta^2)$, and foci at $u_{1,i}^F = -c\eta(1-\eta^2)^{-1}\left(\tau + (-1)^i\sqrt{\tau^2 - \tau_0^2}\right)$, $i = 1, 2$, that tend to $u_{1,1}^F \rightarrow 0$ and $u_{1,2}^F \rightarrow -\infty$, when $\tau \rightarrow \infty$. (c) When η approaches the cutoff condition $(\eta = 1)$ the axis ratio tends to infinity, and the foci as well as the launch point $\mathbf{x}'(t_0)$ approach $u_1 = -\infty$.

Squaring and rearranging (34) leads to

$$[(1-\eta^2)u_1 + c\eta\tau]^2 + (1-\eta^2)u_2^2 = c^2\left(\tau^2 - \tau_0^2\right), \quad (35)$$

$$\tau_0 \equiv \sqrt{1-\eta^2}\frac{z}{c} = t_0 - \frac{\eta\boldsymbol{i}_{u_1}\cdot\mathbf{x}}{c} \quad (36)$$

with $\Re e\sqrt{1-\eta^2} \geq 0$ and $\Im m\sqrt{1-\eta^2} \leq 0$ in accord with $\Im m k_{zpq} \leq 0$ in (13) (since $k_{z00} = \sqrt{k^2(1-\eta^2)}$; see (7) and (13)). In the (u_1, u_2)-plane, (35) defines p, q-*independent* "equal delay" curves in the u_1, u_2 plane, whose shape depends

on the parameters η, τ and τ_0. We now explore the behavior of the solutions for the FW for various p, q-parameter ranges.

Equation (35) describes an ellipse with foci $(u_1, u_2) = (u_{1,i}^F(\tau), 0)$, with $u_{1,i}^F = -c\eta/(1-\eta^2)(\tau + (-1)^i\sqrt{\tau^2 - \tau_0^2})$ and $i = 1, 2$, center $(u_1, u_2) = (-c\eta\tau/(1-\eta^2), 0))$ and axis ratio $c\eta/(1-\eta^2)$, as shown in Fig. 4. At the turn on time $\tau = \tau_0$, the foci coincide and the ellipse reduces to a point at $\mathbf{x}'(t_0) = -c\eta\tau_0(1-\eta^2)^{-1/2}\boldsymbol{i}_{u_1}$. At later time instants, the ellipse becomes larger, with the focus $u_{1,2}^F$ moving along the $-u_1$ direction and the focus $u_{1,1}^F$ moving toward the origin $u_1 = 0$. For the nonphased case $\eta = 0$, the ellipse degenerates into a circle with center fixed at $(u_1, u_2) = (0, 0)$. When approaching cutoff $(\eta \rightarrow 1)$, the axis ratio tends to infinity, and the two foci as well as the launch point $\mathbf{x}'(t_0)$ move to $-\infty$. (For $\eta > 1$, which corresponds to evanescent FW_{00} in the FD, the equal delay contours become hyperbolas (see (35)), of which only the right-hand branch is relevant. Whether TD radiation is now possible under special phase-matched conditions remains to be explored further.)

The u_1-integral in (33) is exactly like that in [1] for a *line array* of dipoles. For $\tau > 0$, the u_2-dependent u_1-values that satisfy (35) are [1, Eq. (13)]

$$u_{1,i}(t) = \frac{-c}{1-\eta^2}\left(\tau\eta + (-1)^i\sqrt{\tau^2 - \tau_\rho^2(u_2)}\right), \quad i = 1, 2,$$

$$\tau_\rho(u_2) = \frac{\sqrt{1-\eta^2}\rho(u_2)}{c} \quad (37)$$

with $\rho(u_2) = \sqrt{z^2 + u_2^2}$. The two real solutions of (37) for $\tau \geq \tau_\rho(u_2)$ coincide at time $\tau = \tau_\rho(u_2)$ which, at the observer, corresponds to the causal (wavefront) arrival time $t_\rho(u_2) = \eta\boldsymbol{i}_{u_1}\cdot\mathbf{x}/c + \sqrt{1-\eta^2}\rho(u_2)/c$ of a signal due to a *smoothly phased infinite line current* along u_1, located at $u_2 = \text{const.}$, with launch point in the $z = 0$ plane at $u_1 = u_{1,1}(t_0) = u_{1,2}(t_0)$. In the moving coordinate system along the excitation wavefront, $\tau_\rho(u_2)$ represents the signal arrival delay that the moving observer encounters with respect to the exciting current impulse located at $u_1 = ct/\eta$ (Fig. 3). For $\tau > \tau_\rho(u_2)$, these solutions separate according to (37) and move toward $u_{1,1}(t) \rightarrow +\infty$ and $u_{1,2}(t) \rightarrow -\infty$ (Fig. 4). For $\tau < \tau_\rho(u_2)$, the two solutions are conjugate complex and do not lie on the integration path; thus the u_1-integral in (33) vanishes for $\tau < \tau_\rho(u_2)$ (causality). The two *causal* contributions corresponding to $u_{1,1}(t)$ and $u_{1,2}(t)$ are determined by using the formula $\delta[f(u_1)] = \delta(u_1 - u_{1,i})|df/du_1|_{u_{1,i}}^{-1}$ when $f(u_{1,i}) = 0$, as in [1, Sec. V-A]. Substituting for $R(u_{1,i}(t))$ from (34) and (37) and simplifying, one obtains what we shall refer to as the causal *solution* for the (pq, i)-indexed TD–FW

$$\hat{A}_{pq,i}^{\text{FW}}(\mathbf{r}, t) = \frac{e^{-j\boldsymbol{\alpha}_{pq}\cdot\mathbf{x}}}{4\pi d_1 d_2}e^{j\bar{\omega}_{pq}\tau}$$

$$\times \int_{-\infty}^{\infty}e^{-j(\boldsymbol{\alpha}_{pq}\cdot\boldsymbol{i}_{u_2})u_2}$$

$$\times \frac{\exp\left[j(-1)^i\frac{c}{1-\eta^2}\boldsymbol{i}_{u_1}\cdot\boldsymbol{\alpha}_{pq}\sqrt{\tau^2 - \tau_\rho^2(u_2)}\right]}{\sqrt{\tau^2 - (\tau_\rho(u_2))^2}}$$

$$\times U(\tau - \tau_\rho(u_2))du_2 \quad (38)$$

in which $\bar{\omega}_{pq}$ is defined in (19), and where $U(\tau) = 1$ or 0 for $\tau > 0$ or $\tau < 0$, respectively. The U function delimits the integration domain to u_2 points with $\tau > \tau_\rho(u_2) = \sqrt{\tau_0^2 + (1 - \eta^2)u_2^2/c^2}$, i.e., between $u_2 = \pm c\sqrt{\tau^2 - \tau_0^2}/\sqrt{1 - \eta^2}$. Therefore, the integral is nonvanishing only in the case of $\tau > \tau_0$. Changing variables to $v = u_2\sqrt{1 - \eta^2}/\left(c\sqrt{\tau^2 - \tau_0^2}\right)$, and adding the $i = 1$ to the $i = 2$ contributions gives

$$
\begin{aligned}
\hat{A}_{pq}^{\mathrm{FW}}(\mathbf{r}, t) &= \sum_{i=1}^{2} \hat{A}_{pq,i}^{\mathrm{FW}} \\
&= \frac{ce^{-j\boldsymbol{\alpha}_{pq}\cdot\mathbf{x}}}{2\pi d_1 d_2 \sqrt{1 - \eta^2}} e^{j\bar{\omega}_{pq}\tau} \\
&\quad \times \int_{-1}^{1} \exp\left[-j\frac{c\sqrt{\tau^2 - \tau_0^2}}{\sqrt{1 - \eta^2}}(\boldsymbol{\alpha}_{pq}\cdot\boldsymbol{i}_{u_2})v\right] \\
&\quad \times \frac{\cos\left[\frac{c}{1-\eta^2}(\boldsymbol{\alpha}_{pq}\cdot\boldsymbol{i}_{u_1})\sqrt{\tau^2 - \tau_0^2}\sqrt{1 - v^2}\right]}{\sqrt{1 - v^2}} dv.
\end{aligned}
$$
(39)

After expressing $\exp(jav) = \cos(av) + j\sin(av)$ and noting that the the odd part of the integrand does not contribute, we recall the formula $(2/\pi)\int_0^1 dv \cos(av)(1 - v^2)^{-1/2}\cos\left[b(1 - v^2)^{1/2}\right] = J_0\left[(a^2 + b^2)^{1/2}\right]$, with J_0 denoting the Bessel function of zeroth-order [14, p. 28]; observing that $(\boldsymbol{\alpha}_{pq}\cdot\boldsymbol{i}_{u_1})^2 + (\boldsymbol{\alpha}_{pq}\cdot\boldsymbol{i}_{u_2})^2 = \alpha_{pq}^2$, we obtain

$$
\begin{aligned}
\hat{A}_{pq}^{\mathrm{FW}}(\mathbf{r}, t) &= \frac{ce^{-j\boldsymbol{\alpha}_{pq}\cdot\mathbf{x}}}{2d_1 d_2 \sqrt{1 - \eta^2}} e^{j\bar{\omega}_{pq}\tau} \\
&\quad \times J_0\left[\tilde{\omega}_{pq}\sqrt{\tau^2 - \tau_0^2}\right] U(\tau - \tau_0)
\end{aligned}
$$
(40)

in which $\tilde{\omega}_{pq}$ is defined in (22). This result, obtained by applying the Poisson summation formula directly to the TD element-by-element field representation, is coincident with that in (26) obtained from the direct Fourier inversion of the FD-FW. The remarks after (26), concerning the "physically observable" TD–FW, apply here as well.

C. Asymptotic Inversion From the FD

1) Local Frequencies and Wavenumbers: The $\hat{A}_{pq}^{\mathrm{FW}}(\mathbf{r}, t)$ behavior of the high-frequency asymptotic evaluation of the FD inversion integral in (1)

$$
\hat{A}_{pq}^{\mathrm{FW}}(\mathbf{r}, t) = \int_{-\infty}^{\infty} F(\omega)e^{-j\hat{\psi}(\omega)} d\omega
$$
(41)

provides additional insight and parameterizes the TD–FW dispersion process. The manipulations here are 2-D generalizations of those carried out in [1] for the line dipole array, and the principal steps are given below. Referring to the last expression for $A_{pq}^{\mathrm{FW}}(\mathbf{r}, \omega)$ in (12), $F(\omega) = 1/(4\pi j d_1 d_2 k_{zpq})$ accounts for the slowly varying amplitude terms in the integrand. The phase is given by

$$
\hat{\psi}(\omega) = \mathbf{k}_{t,pq}\cdot\mathbf{x} + k_{zpq}z - \omega t
$$
(42)

with $\mathbf{k}_{t,pq}$ and $k_{zpq}(\omega)$ defined in (7) and (13), respectively. The dominant contributions to the integral in the high-frequency range arise from the stationary (saddle) points ω_{pq} of $\hat{\psi}(\omega)$, defined by $(d\hat{\psi}/d\omega)|_{\omega_{pq}} = 0$. (For $p = q = 0$, $d\hat{\psi}/d\omega$ is ω-independent and therefore not amenable to saddle point approximation.) For $q \neq 0$, or $p \neq 0$, the real solutions yield the *local instantaneous frequencies* (see Appendix B)

$$
\begin{aligned}
\omega_{pq,i}(\mathbf{r}, t) &= \bar{\omega}_{pq} + (-1)^i \tilde{\omega}_{pq}\frac{\tau}{\sqrt{\tau^2 - \tau_0^2}} \\
i &= 1, 2, \quad \tau > \tau_0
\end{aligned}
$$
(43)

with τ and τ_0 defined in (16) and (23), respectively. Positive and negative frequencies are denoted by $i = 2$ and $i = 1$, respectively. This expression agrees with that obtained via the operation $\omega_{pq,i}(t) = (d/dt)\left[\bar{\omega}_{pq}\tau + (-1)^i\tilde{\omega}_{pq}\sqrt{\tau^2 - \tau_0^2}\right]$ performed directly on the time-dependent phase in (26), after replacing the Bessel function by its large argument asymptotic approximation.

The two instantaneous frequencies of the TD–FW$_{pq}$ in (43) at a given point $\mathbf{r}$ and a given instant t (τ in the moving reference system; see (31)) are real in the causal domain $t > t_0 = \eta\boldsymbol{i}_{u_1}\cdot\mathbf{x}/c + \tau_0$ ($\tau > \tau_0$), increase with mode indexes p, q but decrease with time t, and approach their observer-independent cutoff frequency when $t \to \infty$, (defined by $|k_{t,pq}| = |k|$) (see Fig. 7)

$$
\begin{aligned}
\omega_{pq,i}(t \to \infty) &= \omega_{pq,i}^{\mathrm{cutoff}} \\
&= \bar{\omega}_{pq} + (-1)^i\tilde{\omega}_{pq}, \quad i = 1, 2.
\end{aligned}
$$
(44)

The instantaneous saddle point frequencies $\omega_{pq,i}(t)$ characterize corresponding instantaneous wavenumbers pertaining to the observer located at $\mathbf{r}$ at time t. For specified $\mathbf{r}$, one obtains

$$
k_{pq,i}(t) = \frac{\omega_{pq,i}(t)}{c},
$$
(45)

$$
\mathbf{k}_{t,pq,i}(t) = \eta\frac{\omega_{pq,i}(t)}{c}\boldsymbol{i}_{u_1} + \boldsymbol{\alpha}_{pq}
$$
(46)

$$
\begin{aligned}
k_{zpq,i}(t) &= \sqrt{k_{pq,i}^2(t) - |\mathbf{k}_{t,pq,i}^2(t)|} \\
&= (-1)^i z\frac{(1 - \eta^2)\tilde{\omega}_{pq}}{c^2\sqrt{\tau^2 - \tau_0^2}}
\end{aligned}
$$
(47)

where the wavenumber $k_{zpq,i}(t)$ is calculated using (68). From (14), the corresponding local FW propagation angles denoted for specified $\mathbf{r}$ by $\Theta_{pq,1}(t)$ and $\Phi_{pq,2}(t)$, respectively, become

$$
\begin{aligned}
\cos\Theta_{pq,i}(t) &= \frac{k_{zpq,i}(t)}{k_{pq,i}(t)} \\
&= \frac{\left(\frac{\tau_0}{\tau}\right)\sqrt{1 - \eta^2}}{1 + (-1)^i\frac{\bar{\omega}_{pq}}{\tilde{\omega}_{pq}}\sqrt{1 - \left(\frac{\tau_0}{\tau}\right)^2}}, \quad i = 1, 2
\end{aligned}
$$
(48)

$$
\tan\Phi_{pq,i}(t) = \frac{k_{x2,p,i}(t)}{k_{x1,q,i}(t)}, \quad i = 1, 2.
$$
(49)

Evaluation of the qth TD–FW integral in (41) via the standard asymptotic formula [12, p. 382]

$$
\hat{A}_{pq}^{\mathrm{FW}}(\mathbf{r}, t) \sim \sum_{i=1}^{2} \hat{A}_{pq,i}^{\mathrm{FW}}
$$
(50)

$$
\hat{A}_{pq,i}^{\mathrm{FW}} \sim F(\omega_{pq,i})\frac{\sqrt{2\pi}e^{-j\hat{\psi}(\omega_{pq,i}(t))}}{\sqrt{j\left(\frac{d^2}{d\omega^2}\right)\hat{\psi}|_{\omega_{pq,i}}}}U(\tau - \tau_0)
$$
(51)

yields

$$\hat{A}_{pq,i}^{\mathrm{FW}}(\mathbf{r},t) \sim \frac{ce^{-j\boldsymbol{\alpha}_{pq}\cdot\mathbf{x}}e^{-j(-i)^i\pi/4}}{2d_1 d_2\sqrt{2\pi(1-\eta^2)}}$$
$$\times \frac{e^{j\left(\bar{\omega}_{pq}\tau+(-1)^i\tilde{\omega}_{pq}\sqrt{\tau^2-\tau_0^2}\right)}}{\sqrt{\tilde{\omega}_{pq}}(\tau^2-\tau_0^2)^{1/4}}U(\tau-\tau_0) \quad (52)$$

where we have used (43), (47) and $(d^2/d\omega^2)\hat{\psi}|_{\omega_{pq,i}} = -z(1-\eta^2)^2 c^{-4}\tilde{\omega}_{pq}^2 k_{zpq,i}^{-3} = -(-1)^i c^2(\tau^2-\tau_0^2)^{3/2}/[(1-\eta^2)z^2\tilde{\omega}_{pq}]$. The unit step function $U(\tau-\tau_0)$ arises because real saddle point frequencies $\omega_{pq,i}$ are restricted to $\tau > \tau_0$ $(t > t_0)$. Combining $i = 1$ with $i = 2$ yields

$$\hat{A}_{pq}^{\mathrm{FW}}(\mathbf{r},t) \sim \frac{ce^{-j(\boldsymbol{\alpha}_{pq}\cdot\mathbf{x}-\bar{\omega}_{pq}\tau)}}{d_1 d_2\sqrt{2\pi(1-\eta^2)}}$$
$$\times \frac{\cos\left(\tilde{\omega}_{pq}\sqrt{\tau^2-\tau_0^2}-\frac{\pi}{4}\right)}{\sqrt{\tilde{\omega}_{pq}}(\tau^2-\tau_0^2)^{1/4}}U(\tau-\tau_0). \quad (53)$$

The FD-inverted asymptotic TD–FW in (53) is the asymptotic version of the *exact* TD–FW in (26) obtained through Poisson summation directly in the time domain, as can be seen from the asymptotic approximation of the Bessel functions $J_0(x) \sim \sqrt{2/(\pi x)}\cos(x - \pi/4)$. Thus, all interpretations relating to (26) apply. The fact that *all* TD–FW propagate simultaneously toward the observer is in accord with the instantaneous wavenumber $k_{zpq,i}(t)$ in (47), that is real when $\tau > \tau_0$ for all $p, q = 0, \pm 1, \pm 2, \ldots$. Indeed, the asymptotic frequencies $\omega_{pq,i}(t)$ are such that $|\mathbf{k}_{t,pq,i}(t)| < |\mathbf{k}_{pq,i}(t)|$ whence, after turn-on $(\tau > \tau_0)$, $k_{zpq,i}(t)$ in (47) is real (condition for propagation). At the turn-on time $\tau = \tau_0(t = t_0)$, we have $|\mathbf{k}_{t,pq,i}(t_0)| = \infty$ and $|k_{zpq,i}(t_0)| = \infty$. For $t \to \infty$ we have $\omega_{pq,i}(t \to \infty) = \omega_{pq,i}^{\mathrm{cutoff}}$ (see (44)); thus, the wavenumbers $|\mathbf{k}_{t,pq,i}(t \to \infty)| = |k_{pq,i}(t \to \infty)|$, with $|k_{zpq,i}(t \to \infty)| = 0$, as in the text after (14).

2) The Nondimensional Estimator: In order to assess the accuracy of the asymptotics in (50), we use the *nondimensional estimator* defined as [15]

$$E_s = \left|\frac{F\psi'}{F''}\right|_{\omega_{pq,i}} = |k_{z,pq,i}z|\frac{\tau^2-\tau_0^2}{3\tau^2-\tau_0^2}$$
$$= \tilde{\omega}_{pq}\tau_0 \frac{\sqrt{\left(\frac{\tau}{\tau_0}\right)^2-1}}{3\left(\frac{\tau}{\tau_0}\right)^2-1} \quad (54)$$

which combines the various critical problem parameters and variables. We have noted here that $F''(\omega_{pq,i}) = (1-\eta^2)^2\tilde{\omega}_{pq}^2\left(3\tau^2-\tau_0^2\right)/\left[k_{z,pq,i}^5 c^4(\tau^2-\tau_0^2)\right]$. The range of validity of the asymptotic solution is expressed thereby through the condition $E_s \gg 1$, with the limits given by $E_s \sim O(1)$. As a function of τ, this eliminates the near-wavefront regime $\tau \approx \tau_0$ and the late-time regime $\tau \to \infty$, for both of which $E_s \to 0$. However, the validity of the asymptotic result is extended to $\tau \approx \tau_0$ when the dipoles are excited by a band-limited waveform (see Section V-B).
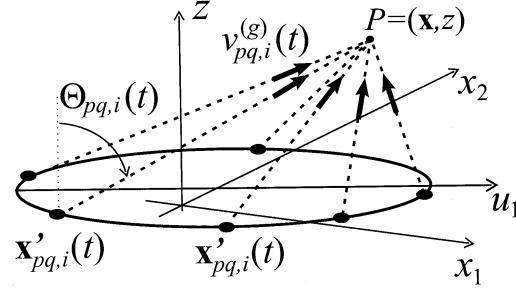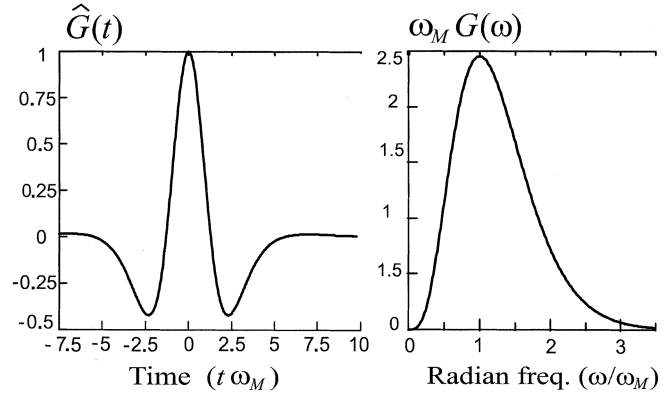

Fig. 5. All TD–FWs propagate *simultaneously* toward the observer with group velocity $\boldsymbol{v}_{pq,i}^{(g)}(t)$, $\left|\boldsymbol{v}_{pq,i}^{(g)}(t)\right| = c$. The emergence point $\mathbf{x}'_{pq,i}(t)$ of each TD–FW$_{pq}$ is located on the t-dependent "equal delay" ellipse defined in (31).

6. Normalized Rayleigh pulse and its FD spectrum.

3) Group Velocity: The group velocity, which specifies the direction and propagation speed of the *energy flux* of the $\hat{A}_{pq}^{\mathrm{FW}}$ wave field, is defined as

$$\boldsymbol{v}_{pq,i}^{(g)} = \left(v_{x1,pq,i}^{(g)}, v_{x2,pq,i}^{(g)}, v_{z,pq,i}^{(g)}\right)$$
$$v_{x1,pq,i}^{(g)} = (\partial\omega(k_{x1},k_{x2},k_z)/\partial k_{x1})|_{pq,i}$$
$$v_{z,pq,i}^{(g)} = (\partial\omega(k_{x1},k_{x2},k_z)/\partial k_z)|_{pq,i}$$

with

$$\omega\left(k_{x1},k_{x2},k_z\right) = c(k_{x1}^2+k_{x2}^2+k_z^2)^{1/2}.$$

Thus, $\partial\omega/\partial k_{x1} = ck_{x1}/k$, $\partial\omega/\partial k_{x2} = ck_{x2}/k$ and $\partial\omega/\partial k_z = ck_z/k$. Inserting the instantaneous wavenumbers from (46) and (47) and using the instantaneous propagation angle $\Theta_{pq,i}(t)$ in (48), yields

$$\boldsymbol{v}_{pq,i}^{(g)} = c\left[\boldsymbol{i}_{x1}\sin\Theta_{pq,i}(t)\cos\Phi_{pq,i}(t)\right.$$
$$+ \boldsymbol{i}_{x2}\sin\Theta_{pq,i}(t)\sin\Phi_{pq,i}(t)$$
$$\left.+ \boldsymbol{i}_z\cos\Theta_{pq,i}(t)\right]i = 1,2. \quad (55)$$

Thus, all instantaneous $\hat{A}_{pq,i}^{\mathrm{FW}}(\mathbf{r},t)$ fields propagate toward the observer with group speed $\left|\boldsymbol{v}_{pq,i}^{(p)}\right| = c$ as shown in Fig. 5.

4) Instantaneous Localization: To complete the connection between the exact and asymptotic results, we show that at the
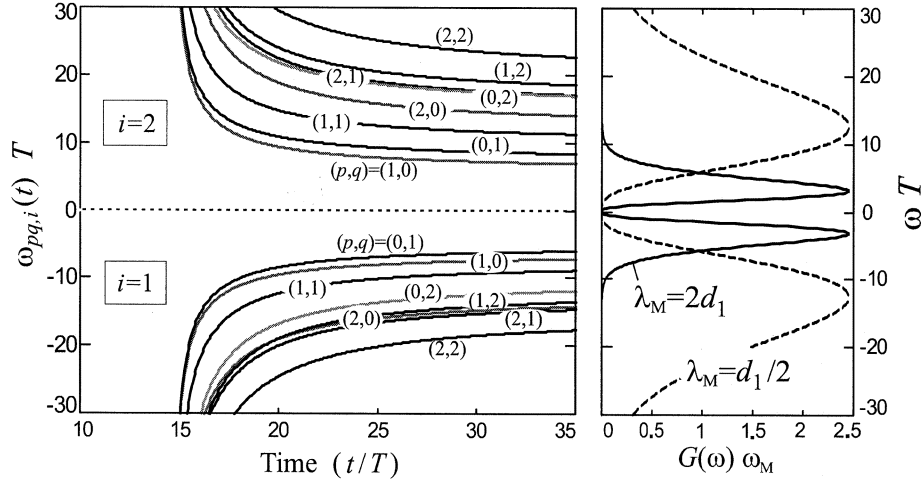
Fig. 7. Local instantaneous radian frequency of oscillation $\omega_{pq,i}(t)$ of the TD–FWs, evaluated at $(x_1, x_2, z) = (0, 0, 15d_1)$, versus normalized time t/T, with $T = d_1/c$. Only those with $|p|, |q| \leq 2$ are shown. Parameters: $d_1 = d_2$; $\eta = 0.2$, $\boldsymbol{i}_{u_1} = \boldsymbol{i}_{x_1}$. At turn-on $t = t_0$, $|\omega_{pq,i}(t)| \to \infty$ for all p, q. At the RHS, pulse-excitation spectra are shown for the two cases analyzed in Fig. 8 ($\omega_M = \pi c/d_1$; $\lambda_M = 2d_1$) and in Fig. 10 ($\omega_M = 4\pi c/d_1$; $\lambda = d_1/2$). In each case, only those TD–FWs with local instantaneous frequency lying within the excitation spectrum are excited.

observation point $(\mathbf{x}, z)$, localization through local instantaneous frequencies and wavenumbers $k_{pq,i}(t)$ and $\mathbf{k}_{t,pq,i}(t)$ in (45) and (46), respectively, define localized "emergence" points

$$\mathbf{x}'_{pq,i}(t) = \mathbf{x} - \mathbf{k}_{t,pq,i}(t) \frac{z}{k_{z,pq,i}(t)} \qquad (56)$$

on the array plane; these points all lie on the t-instantaneous "equal delay" ellipse defined in (31), as shown in Fig. 5. We first recall the definition of $R(\mathbf{x}')$ in (11), and thus $R\left[\mathbf{x}'_{pq,i}(t)\right] = \left[z^2 + z^2|\mathbf{k}_{t,pq,i}(t)|^2/k_{z,pq,i}^2(t)\right]^{1/2} = z|k_{pq,i}(t)/k_{z,pq,i}(t)|$ (see Fig. 5) which, when inserted together with (56) into (31), leads to

$$\frac{c\tau k_{z,pq,i}(t)}{z} + \eta \boldsymbol{i}_{u_1} \cdot \mathbf{k}_{t,pq,i}(t) + k_{pq,i}(t) = 0. \qquad (57)$$

This identity is verified from (45)–(47) and (43), and it represents the equation of the "equal delay" ellipse in terms of instantaneous wavenumbers. In summary, at each time t, *all* p, q TD–FWs propagate toward the observer along t-dependent cones, from directions $\Theta_{pq,i}(t)$, $\Phi_{pq,i}(t)$, with the same group velocity c. These TD–FW emerge earlier from points $\mathbf{x}'_{pq,i}(t)$ located on the "equal delay" ellipse at time t.

D. The Total Physically Observable Radiated Field

The total "physically observable" field radiated by the array is expressed as a sum of $(+p, +q)$, $(-p, -q)$ paired TD–FWs,

$$\hat{A}^{\text{tot}}(\mathbf{r}, t) = \sum_{p,q=-\infty}^{\infty} \hat{A}_{pq}^{\text{FW}}(\mathbf{r}, t) = \sum_{p,q=-\infty}^{\infty} \Re e \hat{A}_{pq}^{\text{FW}}(\mathbf{r}, t) \qquad (58)$$

where the pqth TD–FW $\hat{A}_{pq}^{\text{FW}}$ is given by (26) or (40). The terms in the series on the RHS of (58) can also be rearranged so as to include only positive (and zero) p, q indexes.

V. BAND-LIMITED PULSE EXCITATION

We now analyze the effects of physically realizable band-limited (BL) pulsed dipole excitation on the field radiated by the

planar array. The pulse excitation function is represented as $\hat{G}(t)$ with spectrum $G(\omega)$. Accordingly, the factor multiplying $\delta(\mathbf{x}' - \mathbf{x}_{mn})$ in (2) becomes $G(\omega) \exp(-j\eta k \boldsymbol{i}_{u_1} \cdot \mathbf{x}_{mn})$ for the FD dipole currents and $\hat{G}(t - \eta \boldsymbol{i}_{u_1} \cdot \mathbf{x}_{mn}/c)$ for the TD dipole currents.

The total BL response $\hat{A}^{\text{tot,BL}}(\mathbf{r}, t)$ of the planar array is then obtained by convolving the total TD impulse response in (58) with the BL signal $\hat{G}(t)$, yielding

$$\hat{A}^{\text{tot,BL}}(\mathbf{r}, t) = \sum_{pq=-\infty}^{\infty} \hat{A}_{pq}^{\text{FW,BL}}$$

$$= \sum_{pq=-\infty}^{\infty} \Re e \hat{A}_{pq}^{\text{FW,BL}}, \qquad (59)$$

$$\hat{A}_{pq}^{\text{FW,BL}}(\mathbf{r}, t) = \int_{-\infty}^{\infty} \hat{G}(t') \hat{A}_{pq}^{\text{FW}}(\mathbf{r}, t - t') dt', \qquad (60)$$

The BL Floquet-modulated signal $\hat{A}_{pq}^{\text{FW,BL}}$ due to the planar array can be calculated either by convolution with the exact TD–FW or by inversion of FD asymptotics.

A. Convolution With the Exact FW

Here, the exact FW field in (26) or (40) is used in (60). Again, the $(+p, +q)$, $(-p, -q)$ pairing defines "physisically observable" BL–TD–FW, yielding the real field $\hat{A}_{pq}^{\text{FW,BL}} + \hat{A}_{-p,-q}^{\text{FW,BL}} = 2\Re e \hat{A}_{pq}^{\text{FW,BL}}$, that also demonstrates (59) for BL excitation.

B. Band-Limited Asymptotics

Avoiding the convolution in (60), the pqth BL field $\hat{A}_{pq}^{\text{FW,BL}}$ can be calculated as the inverse Fourier transform of $G(\omega) A_{pq}^{\text{FW}}(\mathbf{r}, \omega)$. Therefore, for p or $q \neq 0$, using the high-frequency asymptotics in Section IV-C, $\hat{A}_{pq}^{\text{FW,BL}}$ can be evaluated approximately by including the pulse spectrum $G(\omega)$ in the inversion integral (41). For these short pulses, $G(\omega)$ can be considered slowly varying with respect to the phase in the integrand of (41) [2], [16], and can therefore be approximated

by its value at the saddle point frequencies $\omega_{pq,i}(t)$, $i = 1, 2$. Thus, near the wavefronts

$$\hat{A}_{pq}^{\mathrm{FW,BL}}(\mathbf{r}, t) = \sum_{i=1}^{2} \hat{A}_{pq,i}^{\mathrm{FW,BL}}(\mathbf{r}, t) \qquad (61)$$

with

$$\hat{A}_{pq,i}^{\mathrm{FW,BL}}(\mathbf{r}, t) \sim G(\omega_{pq,i}(t)) \hat{A}_{pq,i}^{\mathrm{FW}}(\mathbf{r}, t) \qquad (62)$$

and $\widehat{A}_{pq,i}$ approximated asymptotically as in (52). Again, $(+p, +q)$, $(-p, -q)$ pairing synthesizes the real BL asymptotic solution

$$\hat{A}_{pq,2}^{\mathrm{FW,BL}} + \hat{A}_{-p,-q,1}^{\mathrm{FW,BL}} = 2\Re e \hat{A}_{pq,i}^{\mathrm{FW,BL}} \qquad (63)$$

since $G(-\omega) = G^*(\omega)$, $\omega_{-p,-q,1}(t) = -\omega_{pq,2}(t)$ [see (43)], and $\hat{A}_{-p,-q,1}^{\mathrm{FW}} = \left(\hat{A}_{pq,2}^{\mathrm{FW}}\right)^*$. For $p = q = 0$, which is not amenable to ω-domain saddle point asymptotics (see Section IV-C), the pulsed response $\hat{A}_{00}^{\mathrm{FW,BL}}$ is calculated by the convolution in (60). Although the impulsively excited asymptotic wavefields in Section IV-C are valid only for *early times* close to (behind) the wavefronts, convolution with a waveform having a band-limited spectrum $G(\omega)$ may enlarge the range of validity to later observation times behind the wavefront. For p or $q \neq 0$, the relevant TD–FW$_{pq}$ fields are those with $\omega_{pq,i}$ in the $\hat{G}(t)$ signal bandwidth.

C. Illustrative Examples

To check the accuracy of the TD–FW-based BL Green's function algorithm for the impulse-excited planar phased dipole array, we have implemented two numerical examples (see Figs. 8 and 10). The TD asymptotic solution (59), with (61), is compared there with a reference solution obtained via element-by-element summation over the pulsed radiation from all dipoles, i.e.,

$$\frac{\widehat{G}\left(t - \frac{\eta \boldsymbol{i}_{u_1} \cdot \mathbf{x}_{mn}}{c} - \frac{R(\mathbf{x}_{mn})}{c}\right)}{4\pi R(\mathbf{x}_{mn})}, \quad m, n = 0, \pm 1, \pm 2, \ldots. \qquad (64)$$

The mn-series has been truncated when contributions from the far elements are negligible, i.e., when $|m|, |n| < 80$. The chosen BL excitation is a normalized Rayleigh pulse $\widehat{G}(t) = \Re e \left[j/(j + \omega_M t/4)^5\right]$ (i.e., $\widehat{G}(0) = 1$) [17], with FD spectrum $G(\omega) = \pi(6\omega_M)^{-1}(j4\omega/\omega_M)^4 \exp(-4|\omega|/\omega_M)$ and central radian frequency ω_M, shown in Fig. 6.

To explain the results in Figs. 8 and 10, we shall utilize plots of the TD–FW instantaneous frequency dispersions $\omega_{pq,i}(t)$ shown in Fig. 7. The relevant spectral range of $\omega_{pq,i}(t)$ that contributes significantly to the total radiated field at the observer can be assessed from Fig. 7 which shows on the left the instantaneous radian frequency trajectories for $|p|, |q| \leq 2$, evaluated at $(x_1, x_2, z) = (0, 0, 15d_1)$, and plotted versus normalized time t/T, with $T = d_1/c$; the array parameters are $d_1 = d_2$, $\eta = 0.2$ ($\Theta_{00} = 78°$ in (14)), and $\boldsymbol{i}_{u_1} = \boldsymbol{i}_{x_1}$. At turn-on $t = t_0$, all instantaneous frequencies $|\omega_{pq,i}(t)| \to \infty$ with p or $q \neq 0$. It is also seen that for $t \to \infty$, $\omega_{pq,i}(t) \to \omega_{pq,i}^{\mathrm{cutoff}}$ defined in (44). The index $i = 1, 2$ tags negative/positive p, q-frequencies, respectively. The RHS of
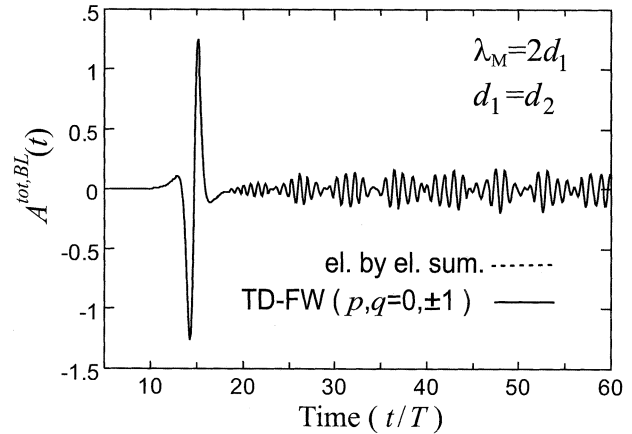

Fig. 8. Field radiated by an infinite planar array of dipoles observed at $(x_1, x_2, z) = (0, 0, 15d_1)$. The fields are plotted versus normalized time t/T, with $T = d_1/c$. Parameters: $d_1 = d_2$; $\eta = 0.2$, $\boldsymbol{i}_{u_1} = \boldsymbol{i}_{x_1}$, $\lambda_M = 2d_1$, $\omega_M = \pi/T$.

Fig. 7, shows the pulse-excitation frequency spectra for the two cases under consideration: $\omega_M = \pi c/d_1$; $\lambda_M = 2d_1$ (Fig. 8) and $\omega_M = 4\pi c/d_1$; $\lambda_M = d_1/2$ (Fig. 10). In each case, only those TD–FWs with instantaneous frequencies $\omega_{pq,i}$ within the excitation spectrum $G(\omega)$ are relevant, as stated in (61),(62).

The fields are likewise plotted versus normalized time t/T, with $T = d_1/c$. Fig. 8 shows the field radiated by the array with parameters $d_1 = d_2$, and $\eta = 0.2$, observed at $x_1 = x_2 = 0$, $z = 15d_1$. The central radian frequency is chosen as $\omega_M = \pi c/d_1$, with central wavelength $\lambda_M = 2\pi c/\omega_M = 2d_1$; this implies from Fig. 7 that the $\omega_{pq,i}(t)$ for only those TD–FWs with $|p|, |q| \leq 1$ lie in the region where $G(\omega)$ is nonvanishing, and therefore furnish the dominant contributions. Indeed, in Fig. 8, excellent agreement with the reference solution has been obtained by retaining only the asymptotic terms $|p|, |q| \leq 1$, thereby demonstrating good convergence of the TD–FW field representation. Since the median wavelength is larger than the interelement spacings ($\lambda_M = 2d_1 = 2d_2$), the main feature of the pulse shape in Fig. 8, is contributed by the integrated excitation waveform of Fig. 6 and represents the TD–FW$_{00}$, which is evaluated by the convolution in (60) [see text after (63)]. The tail after the wavefront is due to the higher order FWs with $|p|, |q| \leq 1$, which oscillate at their distinct local instantaneous frequencies $\omega_{pq,i}(t)$, $i = 1, 2$, $|p|, |q| \leq 1$ and thereby form the noted interference pattern.

The quality of the asymptotic results in Fig. 8 up to $t = 60T$ (and beyond) is assessed by the behavior of the nondimensional estimators $E_{s,pq}(t)$ in (54), as shown in Fig. 9 for $|p|, |q| \leq 2$. The estimator for $p = q = 0$ is not included since FW$_{0,0}$ it is not amenable to saddle point asymptotics as noted in Section IV-C. In the plotted range, $E_{s,pq} \gg 1$ for all t except near turn-on $t = t_0$ ($\tau = \tau_0$) where $E_{s,pq}(t_0) \sim 0$. Near t_0, the local instantaneous frequencies tend to infinity, but due to the band-limited excitation frequency spectrum $G(\omega)$ in Fig. 6, TD–FWs with p or $q \neq 0$ are not excited there.

Fig. 10 shows plots for an infinite planar array under the same conditions as in Fig. 8, except that the central radian frequency is now $\omega_M = 4\pi c/d_1$ ($\lambda_M = 2\pi c/\omega_M = d_1/2$). This changes the relevant spectral range of $\omega_{pq,i}(t)$ to $|p|, |q| \leq$
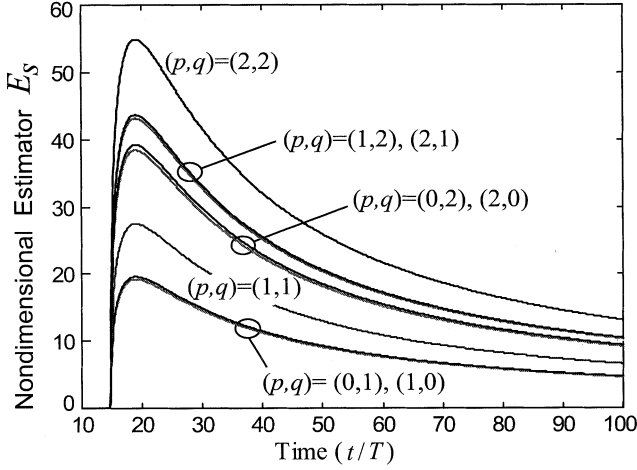
Fig. 9. Nondimensional estimators $E_{s,pq}(t)$ in (54), shown for $|p|, |q| \leq 2$. The quality of the asymptotics for the pqth TD–FW is assessed by how well each satisfies the condition $E_{s,pq} \gg 1$, with respect to an arbitrarily set reference level.
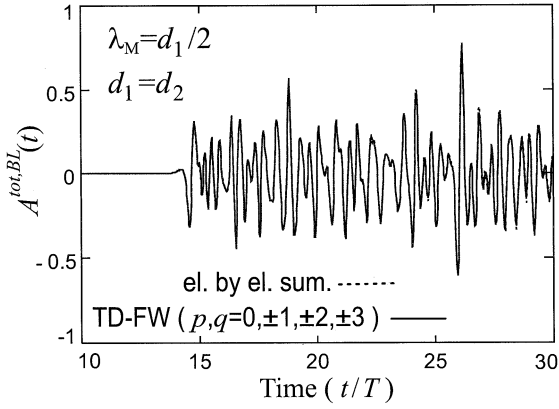

Fig. 10. Field radiated by an infinite planar array of dipoles observed at $(x_1, x_2, z) = (0, 0, 15d_1)$. The fields are plotted versus normalized time t/T, with $T = d_1/c$. Parameters: $d_1 = d_2$; $\eta = 0.2$, $\boldsymbol{i}_{u_1} = \boldsymbol{i}_{x_1}$, $\lambda_M = d_1/2$, $\omega_M = 4\pi/T$.

3, as can be seen from Fig. 7. Accordingly, it is noted that excellent agreement with the reference solution has been obtained also in this case by retaining the relevant asymptotic terms $|p|, |q| \leq 3$, thereby again demonstrating good convergence of the TD–FW field representation. At these shorter wavelengths, features of individual element arrivals become more pronounced but are well synthesized by a correspondingly larger number of TD–FWs.

VI. CONCLUSION

In this paper we have extended previous studies of periodicity-induced impulsive Green's functions for phased arrays of dipoles from the line dipole array (infinite [1] and truncated [2]) to an infinite planar array. From the detailed analyses in [1] and [2], we have gained substantial insight into relevant techniques for quantifying and interpreting TD periodicity-induced global phenomena in terms of TD–FW wavefields. The new features introduced by the assembly of an infinite periodic array in terms of phased line dipole arrays in Section IV-B therefore

bear strong *notational* resemblance to the FD planar array sector geometry in [5], and strong *phenomenological* resemblance to that of the TD infinite line dipole array in [1]. To highlight these analogies, we have used phrasings similar to those in [1] and [2] for similar concepts and methodologies. As in [1], the present prototype problem is sufficiently simple to yield the exact closed form TD solutions in (28) for Floquet-type *dispersive* wave phenomena, which are dispersive TD–FW radiating *plane waves* for $\eta < 1$; the nonradiating case $\eta > 1$ will be presented separately. The most interesting and new finding here is the excitation mechanism (for $\eta < 1$) of the TD–FWs along "equal delay" ellipses in the array plane (see (35) and Figs. 3 and 4), and the appealing physical interpretations that follow from it (see Fig. 5). The next prototype studies will be of the TD–GFs for a semiinfinite planar [18], and thereafter for a plane-sectoral, phased dipole array. This will furnish the tools for analyzing actual finite planar arrays under short pulse conditions. The practical utility of FW-based dipole GFs for finite planar phased arrays has already been demonstrated in the frequency domain [3]–[10], and application of its TD counterpart will be guided by these FD studies.

APPENDIX A

DETAILS PERTAINING TO (25)

We perform the change of variable $\zeta = \sqrt{\omega'^2 - \tilde{\omega}_{pq}^2}$ in the integral in (25). Along the paths P_1 and P_2 in Fig. 2, the variable ζ assumes real values from $-\infty$ to ∞, and the inverse is defined as $\omega' = -(-1)^i \sqrt{\zeta^2 + \tilde{\omega}_{pq}^2}$ with $i = 1, 2$ when ω' is on $P_{1,2}$, respectively. The integral in (25) is thus rewritten as

$$I_i = -(-1)^i \int_{-\infty}^{\infty} d\zeta e^{-j\zeta\tau_0} \frac{e^{-(-1)^i j\tau \sqrt{\zeta^2 + \tilde{\omega}_{pq}^2}}}{\sqrt{\zeta^2 + \tilde{\omega}_{pq}^2}}$$

$$= \pi j H_0^{(i)} \left[|\tilde{\omega}_{pq}| \sqrt{\tau^2 - \tau_0^2} \right] \qquad (65)$$

which has been recognized as a zeroth-order Hankel function of the first or second kind when $i = 1$ or $i = 2$, respectively [12, p. 493], thereby establishing (25).

APPENDIX B

DETAILS PERTAINING TO (43)

Recalling (42), the saddle point condition $d\hat{\psi}/d\omega = 0$ is

$$\frac{(1 - \eta^2)k - \eta(\boldsymbol{\alpha}_{pq} \cdot \boldsymbol{i}_{u_1})}{k_{zpq}} \frac{z}{c} - \tau = 0, \quad \tau = t - \frac{\eta \boldsymbol{i}_{u_1} \cdot \mathbf{x}}{c}. \qquad (66)$$

Note that $\Re e(k_{zpq}) \geq 0$ or ≤ 0 for $\omega > 0$ or < 0, respectively, in order to satisfy the radiation condition at $z = \infty$ for all ω. Squaring and rearranging yields, using (13)

$$\omega^2 A - 2\omega \bar{\omega}_{pq} A - \left[\bar{\omega}_{pq}^2 \tau_0^2 + \frac{\alpha_{pq}^2 c^2 \tau^2}{1 - \eta^2} \right] = 0 \qquad (67)$$

with $A = (\tau^2 - \tau_0^2)$. After recalling that $\tilde{\omega}_{pq} = \bar{\omega}_{pq} + \alpha_{pq}^2 c^2/(1 - \eta^2)$, (67) has the two i-indexed solu-

tions in (43). To sort out the correct solution for $\eta \triangleq 1$, we substitute (43) into the original (66) [recalling(13)] to obtain

$$(-1)^i \frac{\tilde{\omega}_{pq}\tau_0^2}{\sqrt{\tau^2 - \tau_0^2}} = k_{zpq,i}z, \quad i = 1, 2. \tag{68}$$

Real values of $\omega_{pq,i}$ in (43) are obtained only for $|\tau| > \tau_0$. Since, $(\tau^2 - \tau_0^2)^{1/2} < |\tau|$, the sign of $\omega_{pq,i}$ depends on i through the sign of the second term inside the parentheses in (43), i.e., $\mathrm{sgn}(\omega_{pq,i}) = (-1)^i\mathrm{sgn}(\tilde{\omega}_{pq}\tau)$. Since $\mathrm{sgn}(\Re e k_{zpq}) = \mathrm{sgn}(\omega)$, we have $\mathrm{sgn}(\Re e k_{zpq,i}) = (-1)^i\mathrm{sgn}(\tilde{\omega}_{pq}\tau)$. Thus, both the LHS and RHS of (68) have the same sign for $\tau > \tau_0$ and opposite sign for $\tau < -\tau_0$, for $i = 1, 2$. This means that for $\tau > \tau_0$ both $\omega_{pq,1}$ and $\omega_{pq,2}$ are real solutions of (66), while neither is a solution for negative $\tau < -\tau_0$.

REFERENCES

[1] L. B. Felsen and F. Capolino, "Time domain Green's function for an infinite sequentially excited periodic line array of dipoles," *IEEE Trans. Antennas Propagat.*, vol. 48, pp. 921–931, June 2000.

[2] F. Capolino and L. B. Felsen, "Frequency and time domain Green's functions for a phased semi-infinite periodic line array of dipoles," *IEEE Trans. Antennas Propagat.*, vol. 50, pp. 31–41, Jan. 2002.

[3] F. Capolino, M. Albani, S. Maci, and L. B. Felsen, "Frequency domain Green's function for a planar periodic semi-infinite dipole array. Part I: Truncated Floquet wave formulation," *IEEE Trans. Antennas Propagat.*, vol. 48, pp. 67–74, Jan. 2000.

[4] ——, "Frequency domain Green's function for a planar periodic semi-infinite dipole array. Part II: Phenomenology of diffracted waves," *IEEE Trans. Antennas Propagat.*, vol. 48, pp. 75–85, Jan. 2000.

[5] F. Capolino, S. Maci, and L. B. Felsen, "Asymptotic high-frequency Green's function for a planar phased sectoral array of dipoles," in *Proc. Radio Science-Invited Paper*, vol. 35, Ser. Special Issue 1998 URSI Int. Symp. Electromagn. Theory, Mar.–Apr. 2000, pp. 579–593.

[6] S. Maci, F. Capolino, and L. B. Felsen, "Three dimensional Green's function for planar rectangular phased dipole arrays," in *Proc. Wave Motion-Invited Paper*, vol. 34, Special Issue on Electrodynamics in Complex Environments, Sept. 2001, pp. 263–279.

[7] A. Neto, S. Maci, G. Vecchi, and M. Sabbadini, "Truncated Floquet wave diffraction method for the full wave analysis of large phased arrays. Part I: Basic principles and 2D case," *IEEE Trans. Antennas Propagat.*, vol. 48, pp. 594–600, Apr. 2000.

[8] ——, "Truncated Floquet wave diffraction method for the full wave analysis of large phased arrays. Part II: Generalization to the 3D case," *IEEE Trans. Antennas Propagat.*, vol. 48, pp. 600–611, Apr. 2000.

[9] A. Cucini, M. Albani, and S. Maci, "Truncated Floquet wave full wave (T(FW)2) analysis of large periodic arrays of rectangular waveguides, in print for," IEEE Trans. Antennas Propagat., vol. 50, 2002.

[10] F. Capolino, S. Maci, M. Sabbadini, and L. B. Felsen, "Large phased arrays on complex platforms," in Proc. Int. Conf. Electromagnetics and Advanced Appl. (ICEAA), Torino, Italy, Sept. 10–14, 2001.

[11] A. Papoulis, *Systems and Transforms With Application in Optics*. Malabar, FL: R.E. Krieger, 1981.

[12] L. B. Felsen and N. Marcuvitz, *Radiation and Scattering of Waves*. Englewood Cliffs, NJ: Prentice-Hall, 1973.

[13] S. R. Deans, *The Radon Transform and Some of Its Applications*. Malabar, FL: R. E. Krieger, 1993.

[14] A. Erdélyi *et al.*, *Tables of Integral Transforms*. New York, Canada, England: McGraw-Hill, 1954, vol. I.

[15] L. B. Felsen, "Complexity architecture, phase space dynamics and problem-matched Green's functions," in *Wave Motion-Invited Paper*, vol. 34, Special Issue on Electrodynamics in Complex Environments, Sept. 2001, pp. 243–262.

[16] L. B. Felsen and L. Carin, "Diffraction theory of frequency- and time-domain scattering by weakly aperiodic truncated thin-wire gratings," *J. Opt. Soc. Amer. A*, vol. 11, no. 4, pp. 1291–1306, Apr. 1994.

[17] P. Hubral and M. Tygel, "Analysis of the rayleigh pulse," *Geophysics*, vol. 54, no. 5, pp. 654–658, May 1989.

[18] F. Capolino and L. B. Felsen, "Short-pulse radiation by a sequentially excited semi-infinite periodic planar array of dipoles," in *Radio Science-Invited Paper*, Ser. Special Issue 2001 URSI Int. Symp. Electromagn. Theory, Mar.-Apr. 2003.

Filippo Capolino (S'94–M'97) was born in Florence, Italy, in 1967. He received the *Laurea* degree (*cum laude*) in electronic engineering and the Ph.D. degree, from the University of Florence, Italy, in 1993 and 1997, respectively.

From 1994 to 2000, he was been a lecturer of antennas at the Diploma di Laurea, University of Siena, Italy, where he was also a Research Associate. From 1997 to 1998, he was a Fulbright Research Visitor with the Department of Aerospace and Mechanical Engineering, Boston University, Boston, MA, where he continued his research with a Grant from the Italian National Council for Research (CNR), from 1998 to 1999. He is currently a research associate visiting professor with the Department of Electrical and Computer Engineering, University of Houston, Houston, TX. His research interests include theoretical and applied electromagnetics focused on high-frequency short-pulse radiation, array antennas, periodic structures, and numerical modeling.

Dr. Capolino was awarded with a MMET'94 Student Paper Competition in 1994, the Raj Mittra Travel Grant for Young Scientists in 1996, the "Barzilai" prize for the best paper at the National Italian Congress of Electromagnetism (XI RiNEm) in 1996, and a Young Scientist Award for participating at the URSI Int. Symp. Electromagn. Theory in 1998. He received the R. W. P. King Prize Paper Award from the IEEE Antennas and Propagation Society for the Best Paper of the Year 2000, by an author under 36 years old.

Leopold B. Felsen (S'47–M'54–SM'55–F'62–LF'90) was born in Munich, Germany, on May 7, 1924. He received the B.E.E., M.E.E., and D.E.E. degrees from the Polytechnic Institute of Brooklyn, Brooklyn, NY, in 1948, 1950, and 1952, respectively.

He emigrated to the United States in 1939 and served in the U.S. Army from 1943 to 1946. After 1952, he remained with the Polytechnic (now Polytechnic University), gaining the position of University Professor in 1978. From 1974 to 1978, he was Dean of Engineering. In 1994, he resigned from the full-time Polytechnic faculty and was granted the status of University Professor of Emeritus. He is now Professor of Aerospace and Mechanical Engineering and Professor of Electrical and Computer Engineering at Boston University, Boston, MA. He is the author or coauthor of more than 300 papers and of several books, including the classic *Radiation and Scattering of Waves* (Piscataway, NJ: IEEE Press, 1994). He is an Associate Editor of several professional journals and an editor of the *Wave Phenomena Series* (New York: Springer-Verlag). His research interests encompass wave propagation and diffraction in complex environments and in various disciplines, high-frequency asymptotic and short-pulse techniques, and phase-space methods with an emphasis on wave-oriented data processing and imaging.

Dr. Felsen is a Member of Sigma Xi and a Fellow of the Optical Society of America and the Acoustical Society of America. In 1974, he was an IEEE IAPS (Antennas and Propagation Society) Distinguished Lecturer. He has held Visiting Professorships and Fellowships at universities in the United States and abroad, including the Guggenheim in 1973 and the Humboldt Foundation Senior Scientist Award in 1981. He was awarded the Balthasar van der Pol Gold Medal from the International Union of Radio Science (URSI) in 1975, an honorary doctorate from the Technical University of Denmark in 1979, the IEEE Heinrich Hertz Gold Medal for 1991, the APS Distinguished Achievement Award for 1998, the IEEE Third Millenium Medal in 2000 (nomination by APS), three Distinguished Faculty Alumnus Awards from Polytechnic University, and an IEEE Centennial Medal in 1984. Also, awards have been bestowed on several papers authored or coauthored by him. In 1977, he was elected to the National Academy of Engineering. He has served on the APS Administrative Committee from 1963 to 1966, and as Vice Chairman and Chairman for both the United States (1966–1973) and the International (1978–1984) URSI Commission B.